PNAS RESEARCH ARTICLE | IMMUNOLOGY AND INFLAMMATION

DNA hypomethylation ameliorates erosive inflammatory arthritis by modulating interferon regulatory factor-8

Gaurav Swarnkar[a], Nicholas P. Semenkovich[b], Manoj Arra[c], Dorothy K. Mims[a], Syeda Kanwal Naqvi[a], Timothy Peterson[b,d], Gabriel Mbalaviele[b], Chia-Lung Wu[e], and Yousef Abu-Amer[a,f,g,1]

Edited by Georg Schett, University of Erlangen-Nuremberg, Erlangen, Germany; received June 22, 2023; accepted January 8, 2024 by Editorial Board Member Carl F. Nathan

Epigenetic regulation plays a crucial role in the pathogenesis of autoimmune diseases such as inflammatory arthritis. DNA hypomethylating agents, such as decitabine (DAC), have been shown to dampen inflammation and restore immune homeostasis. In the present study, we demonstrate that DAC elicits potent anti-inflammatory effects and attenuates disease symptoms in several animal models of arthritis. Transcriptomic and epigenomic profiling show that DAC-mediated hypomethylation regulates a wide range of cell types in arthritis, altering the differentiation trajectories of anti-inflammatory macrophage populations, regulatory T cells, and tissue-protective synovial fibroblasts (SFs). Mechanistically, DAC-mediated demethylation of intragenic 5'-Cytosine phosphate Guanine-3' (CpG) islands of the transcription factor Irf8 (interferon regulatory factor 8) induced its re-expression and promoted its repressor activity. As a result, DAC restored joint homeostasis by resetting the transcriptomic signature of negative regulators of inflammation in synovial macrophages (MerTK, Trem2, and Cx3cr1), T_{REGs} (Foxp3), and SFs (Pdpn and Fapα). In conclusion, we found that Irf8 is necessary for the inhibitory effect of DAC in murine arthritis and that direct expression of Irf8 is sufficient to significantly mitigate arthritis.

arthritis | Irf8 | decitabine | osteolysis | methylation

Significance

Inflammatory arthritis (IA) is characterized by dysregulation of immune cells that leads to joint swelling, pain, and tissue breakdown. Therefore, understanding the mechanisms underlying this pathology will advance therapeutic interventions. Recent work has suggested that inflammation is governed by dysregulation of DNA methylation, an epigenetic mechanism that regulates gene expression. In this study, we show that the clinically approved hypomethylation drug decitabine (DAC) inhibits murine IA. Furthermore, using transcriptomic screening, we identify the transcription factor interferon regulatory factor 8 (Irf8) as a key component of this mechanism. Specifically, DAC induces expression of Irf8, and direct transduction of Irf8 ameliorates murine IA. These findings position DAC and Irf8 as potential IA therapeutic targets.

Chronic inflammation and autoimmune diseases are often characterized by persistent myeloid activation and proinflammatory output occurring at the level of hematopoietic stem and primitive myeloid progenitor cells. These cells acquire enhanced in vitro and in vivo propensity to generate inflammatory myeloid cells, the key perpetrators of tissue damage in arthritis (1, 2). This hyper-myelopoiesis (and often neutrophilia) that is prevalent in inflammatory joint diseases may be a consequence of dysregulated epigenetic programs and inflammation-mediated silencing of repressor genes. Epigenetic regulation, especially through DNA methylation that alters transcriptional accessibility, plays a key role in joint homeostasis and in pathologic states including inflammatory arthritis (IA) (3–6). Alterations in epigenetic state and transcriptional accessibility have emerged as a critical modulator in various cells in a range of inflammatory diseases, including in synovial fibroblasts (SFs), immune cells, and peripheral blood mononuclear cells (7–15).

Studies of myeloid malignancies led to the discovery of agents targeting methylation, including the cytidine analog 5-aza-2-deoxycytidine [decitabine, Dacogen® (DAC)] (16, 17), which can demethylate previously silenced tumor suppressor genes leading to their reactivation. DAC causes DNA demethylation by inactivation of DNA methyltransferase-1 (DNMT1), the enzyme responsible for methylation (18, 19). At high doses, DAC exposure leads to the formation of covalent adducts between DAC and DNMT1, causing arrest of DNA synthesis in proliferating cells and cell death (17, 20). However, at low nanomolar doses, these adducts are degraded by the proteosome, and DNA synthesis is resumed in the absence of DNMT1 (21). Consequently, proliferating cells are hypomethylated, and previously silenced genes are re-expressed (16, 17, 20). DAC is an approved therapy for the treatment of myelodysplastic syndrome (MDS) and acute myeloid leukemia (22, 23). Approximately 50% of MDS patients demonstrate a clinical response after DAC treatment, with myelosuppression as a major adverse effect (24). Notably, inactivation of certain gene repressors, such as interferon regulatory factor 8 (Irf8), leads to development of chronic myeloid leukemia, characterized by myeloproliferation and systemic expansion of neutrophils (25).

Work in recent years has identified a family of interferon-regulatory factors (IRFs) as key regulators of myeloid lineage determination (26–31). In particular, gene deletion studies have shown that Irf8 plays a prominent role in myelopoiesis (32). Irf8 expression is negligible in early hematopoietic progenitors and increases during differentiation in common/granulocyte myeloid progenitor (CMP/GMPs) fraction (29, 33). High expression of Irf8 was

Author contributions: G.S., C.-L.W., and Y.A.-A. designed research; G.S., N.P.S., M.A., D.K.M., and S.K.N. performed research; G.S., N.P.S., T.P., G.M., C.-L.W., and Y.A.-A. analyzed data; Y.A.-A. funding acquision; and G.S., N.P.S., C.-L.W., and Y.A.-A. wrote the paper.

The authors declare no competing interest.

This article is a PNAS Direct Submission. G.S. is a guest editor invited by the Editorial Board.

Copyright © 2024 the Author(s). Published by PNAS. This article is distributed under Creative Commons Attribution-NonCommercial-NoDerivatives License 4.0 (CC BY-NC-ND).

[1]To whom correspondence may be addressed. Email: abuamery@wustl.edu.

This article contains supporting information online at https://www.pnas.org/lookup/suppl/doi:10.1073/pnas.2310264121/-/DCSupplemental.

Published February 6, 2024.

found in monocyte-DC progenitors (MDPs) and common monocyte progenitors (cMoPs) (34, 35) limiting their proliferation, and *Irf8*−/− mice display an increased number of MDPs, cMoPs, and osteoclasts and develop osteoporosis (36, 37). Most importantly, Irf8 inhibits neutrophil development while *Irf8*−/− mice exhibit severe neutrophilia (30). Mechanistically, Irf8 inhibits neutrophilia by directly binding C/EBPα (the transcription factor that promotes neutrophil differentiation) and blocking C/EBPα chromatin binding and transactivation of target genes. Interestingly, binding of C/EBPα to target genes is facilitated by the methyl group found in the gene promoters (30, 38). Thus, hypermethylated Irf8 loses its suppressive activity facilitating neutrophilia, inflammatory myeloid proliferation, and hyper-osteoclastogenesis (37).

In this study, using assay for whole-genome bisulfite sequencing (WGBS), unsupervised single-cell RNA sequencing (scRNA-seq), and fluorescence-activated cell sorting (FACS) analyses, we report that the demethylating drug DAC reverses inflammation-induced epigenetic, transcriptomic, and cellular changes in immune and nonimmune synovial cells. Furthermore, DAC activates cellular suppressors, primarily Irf8, to attenuate inflammation and erosion in joints of murine models of IA.

Results

The Hypomethylating Agent DAC Ameliorates IA and Modifies Synovial Cell Populations. The pathology of arthritis features distal joint swelling, synovitis, and synovial tissue destruction. Intraperitoneal administration of a low dose of DAC (0.12 mg/kg) dramatically reduced clinical score and inhibited distal joint swelling when administered therapeutically after disease onset (Fig. 1 *A* and *B* and *SI Appendix*, Fig. S1 *A* and *C*) or prophylactically (*SI Appendix*, Fig. S1*B*) in STIA (serum transfer-induced arthritis), collagen-induced arthritis (CIA), and collagen antibody-induced arthritis (CAIA) models. Given that NF-kB activation is an indicator of inflammation in arthritis (39–41), the inflammatory index of IA was measured in RelA NF-κB reporter mice demonstrating that DAC significantly inhibited RelA-Luciferase activity in a dose-dependent manner (*SI Appendix*, Fig. S1 *D* and *E*).

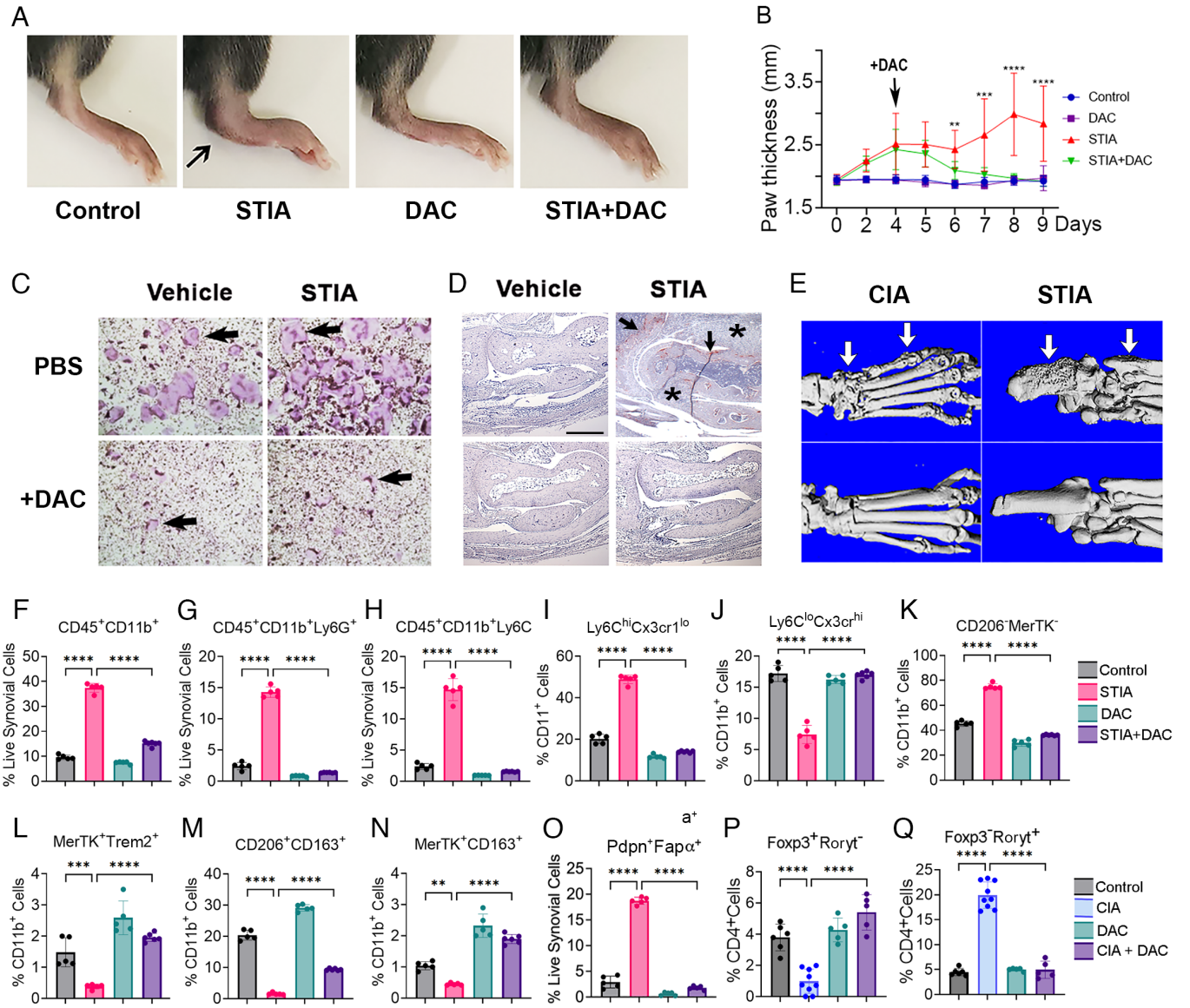

Fig. 1. Low dose of DAC inhibits IA. (*A* and *B*) Paw images and thickness measurements of therapeutically treated STIA mice. Two-way ANOVA, N = 10; ****P< 0.001(STIA vs. STIA + DAC). (*C–E*) Ex-vivo osteoclastogenesis, IHC TRAP-staining, and 3D μCT reconstruction of paws from CIA and STIA mice ± DAC. Error bars represent mean ± SD. One-way ANOVA *P < 0.05, **P < 0.01, ***P < 0.001, and ****P < 0.0001, unless otherwise indicated. (*F–Q*) Multichannel FACS analysis of synovial cells from IA distal joints ± DAC (0.12 mg/kg bw).

Because IA is complicated by joint erosion with notably elevated osteoclastogenesis, these parameters were examined in vivo and ex vivo. To this end, osteoclast progenitors isolated from STIA mouse joints and bone marrow differentiated more readily and with higher propensity into multinucleated osteoclasts when cultured ex vivo, whereas DAC nearly completely halted osteoclastogenesis (Fig. 1*C*). Corroborating these findings, immunohistochemistry tartrate-resistant acid phosphatase (TRAP) staining of joint sections showed dramatic reduction of osteoclasts in DAC-treated STIA mice (Fig. 1*D*; arrows), and mitigated inflammation (Fig. 1*D*; asterisks). Further, μCT analysis showed that DAC significantly protected against bone erosion (Fig. 1*E*; arrows). Buttressing the relevance of these outcomes to joint function, mouse behavioral and pain sensitivity measurements demonstrated that the joint function of DAC-treated mice is similar to control counterparts (*SI Appendix*, Fig. S1 *F–M*). Considering the potential adverse effects of this drug, DAC at the highest dose tested (250 nM) had a negligible effect on BMM and T cell cycle compared with cell cycle arrest at 1% FBS (*SI Appendix*, Fig. S1 *N* and *O*). Critically, there were no significant changes in mouse body weight at a dose triple the optimal dose (0.25 mg/kg) we routinely used (*SI Appendix*, Fig. S1*P*), suggesting that therapeutic dosing of DAC does not lead to systemic cytotoxic effects.

Because IA synovitis is dominated by hyper-myeloproliferation, enhanced circulating proinflammatory ($MHCII^+Ly6C^+$) macrophages (MΦ), and neutrophilia ($CD11b^+Ly6G^+$), the frequency of synovial cells in paws was quantified. FACS analysis revealed that overall $CD11b^+$ population and $Ly6G^{hi}$, $Ly6C^{hi,}$ and $Cx3cr1^{lo}$ subpopulations were increased, whereas frequency of resident synovial MΦ expressing Cx3cr1, MerTK, Trem2, CD163 and the anti-inflammatory MΦ-like cell type markers CD206 and CD163 were reduced at peak arthritis (Fig. 1 *F–N*). Intraperitoneal administration of low doses of DAC was sufficient to reverse synovial cellular changes highlighted by reduced frequency of overall $CD11b^+$ myeloid population, granulocytes/neutrophils ($Ly6G^+$), inflammatory $Ly6C^+$ MΦ, $MerTK^-$ inflammatory MΦ, $MHCII^+$/$MHCII^-$ macrophage ratio, and increased (or gained) frequency of $Cx3cr1^{hi}$, $MerTK^+$ and $CD163^+$ anti-inflammatory MΦ (Fig. 1 *F–N* and *SI Appendix*, Fig. S2 *A–C*). Furthermore, recognizing that SFs and T cells play key roles in IA pathogenesis, the frequency and subtypes of these cells were monitored in IA and IA+DAC joints with FACS analysis using STIA, CIA, and CAIA mouse models. Whereas activated SFs were highly elevated in CIA and CAIA, DAC inhibited CIA- and CAIA-associated activation of SF resident cells underscored by a significant decrease in $Pdpn^+$ $Fap\alpha^+$ inflammatory SFs in the synovial joints (Fig. 1*O*). Further, DAC increased T_{REG} ($Foxp3^+$ $Ror\gamma t^-$) and inhibited T_H17 ($Foxp3^-$ $Ror\gamma t^+$) cells in CIA (Fig. 1 *P* and *Q*) and CAIA (*SI Appendix*, Fig. S2 *D–F*), consistent with recently published reports (42, 43).

STIA Mice Exhibited Significantly Increased Myeloid Clusters, while DAC Drug Treatment Remarkably Reduced Inflammatory Myeloid Populations in Joint Synovium of STIA Mice. To further understand how DAC modulates arthritis, we examined the transcriptional profile of synovial cells derived from control and STIA mice in the absence or presence of DAC. Employing scRNA-seq, normalized gene counts from each of the four experimental groups were evaluated using principal component analysis. We observed that samples within each group (n = 3 samples/group) clustered together, validating consistent transcriptional profile among replicates within each experimental group (*SI Appendix*, Fig. S3). Hierarchical clustering analysis of STIA + DAC samples demonstrated a similar gene expression profile to control samples when compared to STIA-nontreated samples (*SI Appendix*, Fig. S4). This result implies that DAC treatment alters the transcriptional profile of STIA mice reflecting their nondiseased controls more closely. Next, we interrogated the effect of DAC treatment on synovial cell subpopulations. Unsupervised scRNA-seq analysis revealed that control and DAC-treated groups had 3 and 2 myeloid cell clusters, respectively. STIA mice exhibited 9 myeloid cell populations which were significantly reduced to 5 myeloid cell subsets when STIA mice received DAC drug treatment (i.e., STIA + DAC group; *SI Appendix*, Figs. S5–S8*B*). Myeloid cells were identified by conventionally used cell markers including Mrc1, Trem2, S100a8, Adgre1, Retnla, and Napsa (44). In addition, other immune cells such as B cells, T cells, and neutrophils as well as fibroblasts were also detected and annotated according to their corresponding markers (*SI Appendix*, Figs. S5–S8*C*). Unique cell populations in the different clusters in each experimental condition depicted in *SI Appendix*, Figs. S5–S8 are summarized in *SI Appendix*, Table S1. Evaluating distinct cell populations (including myeloid cells, fibroblasts, B cells, T cells, NK cells, and endothelial cells) resulting from experimental conditions (*SI Appendix*, Fig. S9) shows that when compared to control mice, the percentage of myeloid cells in the joint synovium was significantly increased in the STIA mice (~3.2-fold increase), and it was decreased by the DAC treatment (i.e., STIA + DAC). Remarkably, more than 80% of synovial cells in the STIA mice were myeloid cells. The percentages of the rest of synovial cell populations such as fibroblasts, B cells, T cells, and endothelial cells were decreased in the STIA mice compared with control mice (*SI Appendix*, Fig. S9) (Table 1).

Integrative Analysis Identified 12 Distinct Myeloid Cell Populations in the Synovium. Immune cells are pivotal constituents of the inflammatory response. To delineate how inflammation and DAC treatment modulate innate immune myeloid cell phenotypes in joint synovium, we subsetted and integrated myeloid cell clusters detected from control, STIA, and STIA + DAC mice. Unsupervised scRNA-seq analysis using canonical correlations analysis (CCA) identified 12 unique myeloid cell populations in the synovium across three experimental mouse groups: 1) proinflammatory *Wfdc21/Rdh12/Lcn2*$^+$ MΦ, 2) proinflammatory *Tnf/Csf1/Clec4n*$^+$ MΦ, 3) anti-inflammatory *C1qa/Mrc1/Pf4*$^+$ MΦ, 4) anti-inflammatory *Spp1/Cd36/Arg1*$^+$ MΦ, 5) *Chil3/Plac8/Ly6c2*$^+$ Mo, 6) antigen-presenting *Krld1/H2-Aa/Clec10a*$^+$ Mo-DCs, 7) profibrotic *Gm26917/Sparc/Col3a1*$^+$ MΦ, 8) proinflammatory IFN-induced *Gm13822/lift3/Isg15*$^+$ MΦ, 9) TAM-like *Nrp2/Stmn1/Atpif1*$^+$ MΦ, 10) *Wdfy4/Trim35/Irf8*$^+$ Mo-Dc/Neu, 11) tissue-resident *Lyz1/Mgl2/Clec4b1*$^+$ MΦ, and 12) proliferating *Mpo/Ngp/Ctsg*$^+$ MΦ. (Fig. 2 *A–C* and *SI Appendix*, Fig. S10). To identify which of our MΦ populations may belong to osteoclasts and/or are involved in proinflammatory signaling, we generated violin plots focused on key osteoclast genes (*Acp5*, *Ctsk*, *Tnfrsf11a*, *Fos*, *Prdm1/Blimp1*, *Nfatc1*, *Mmp9,* and *Dcstamp*) and NF-κB pathway genes (*Rela*, *Nfkb1,* and *Il1b*) (Fig. 2*D*). It appears that Nrp2/Stmn1/Atpif1$^+$ MΦ had high expression of osteoclast genes, suggesting these cells may be associated with osteoclast lineages. Consistent with our previous findings, proinflammatory MΦ populations (particularly, Wfdc21/Rdh12/Lcn2$^+$ MΦ and Tnf/Csf1/Clec4n$^+$ MΦ) demonstrated high expression of the genes involved in NF-κB pathway. As expected, inflammation significantly increased myeloid cell numbers in the STIA mice compared to the myeloid cells detected in the control mice. Additionally, four distinct myeloid cell populations (i.e., *Wfdc21/Rdh12/Lcn2*$^+$ MΦ, *Tnf/Csf1/Clec4n*$^+$ MΦ, IFN-induced *Gm13822/lift3/Isg15*$^+$ MΦ, and *Wdfy4/Trim35/Irf8*$^+$ Mo-Dc/Neu) were only detected in STIA and STIA + DAC mice but not in control mice (Fig. 2*E*). Next, we compared changes in the distinct macrophage populations due

Table 1. Labled antibodies used for FACS

Reagent	Cat#	Company
Ly6G BV421	127628	BioLegend
CD101 PE-Cy7	25-1011-82	BioLegend
Cd11b BV510	101263	BioLegend
CD163 APC	17-1631-82	BioLegend
CD206 PE	141706	BioLegend
CD4 BV421	100443	Thermo
CD45 BV650	103151	BioLegend
Cell stainign buffer	420201	BioLegend
CX3CR1 FITC	149020	BioLegend
F4/80 SB600	63-4801-82	BioLegend
FAPa APC	BS-5758R	BioLegend
FCy blocker	101302	BioLegend
Fixable viability dye eFluor™ 780	65-0865-18	Thermo
foxp3 PE	12-5773-82	Thermo
Ikbz PerCP-eFluor 710	46-6801-82	Thermo
Ly6C SB780	128041	Thermo
MerTK PE-Cy7	25-5751-82	Thermo
MHCII APC	107614	Thermo
PDPN PE-Cy7	25-5381-82	Thermo
ROR AF488	53-6981-82	Thermo
Trem2 FITC	MA5-28223	Thermo
True-nuclear™ transcription factor buffer set	424401	Thermo

to experimental conditions (*SI Appendix*, Fig. S11). Consistent with our previous analysis, four distinct myeloid cell populations (i.e., Wfdc21/Rdh12/Lcn2+ MΦ, Tnf/Csf1/Clec4n$^+$ MΦ, IFN-induced Gm13822/lift3/Isg15$^+$ MΦ, and Wdfy4/Trim35/Irf8+ Mo-Dc/Neu; dashed square lines) were significantly increased in STIA mice when compared with control mice. DAC treatment showed a trend toward decreasing the percentage of Wdfy4/Trim35/Irf8$^+$ Mo-Dc/Neu cells in the synovium when compared to STIA treatment. Additionally, control mice had significantly higher synovial cell percentage of proliferative Mpo/Ngp/Ctsg+ MΦ (i.e., enriched in Top2a and Mki67 expression) vs. STIA and STIA mice.

DAC Treatment Significantly Restored Anti-Inflammatory Cell Populations and Decreased Inflammatory Gene Expression: Unique Signatures and Functionality of MΦ Populations. Next, the transcriptomic profiles and functionalities of synovial macrophage populations were further explored. We observed that in STIA, proinflammatory Wfdc21/Rdh12/Lcn2$^+$ MΦ demonstrated high expression of Il1a and Tnf (*SI Appendix*, Fig. S12). GO term analysis indicated that Wfdc21/Rdh12/Lcn2$^+$ proinflammatory MΦ express genes enriched for immune system responses, neutrophil chemotaxis, and response to IL-1 (*SI Appendix*, Fig. S13*A*). IFN-induced *Gm13822/lift3/Isg15*$^+$ MΦ phenotype demonstrated that the cellular response to IFNβ and *Tnf/Csf1/Clec4n*$^+$ MΦ is involved in apoptotic process regulation (*SI Appendix*, Fig. S13*A*). The anti-inflammatory *Spp1/Cd36/Arg1*$^+$ MΦ had high expression in *Arg1*, *Trem2*, and *Vegfa* with moderate *Il6* expression levels, while anti-inflammatory *C1qa/Mrc1/Pf4*$^+$ MΦ were enriched in *Mrc1*. Tissue-resident *Lyz1/Mgl2/Clec4b1*$^+$ MΦ subset had the highest expression levels of *Cd81*, *Cd163,* and *Il10* among all MΦ populations (*SI Appendix*, Fig. S12). In GO term functional analysis, *C1qa/Mrc1/Pf4*$^+$ MΦ demonstrated chemotaxis, endocytosis, regulation of ERK cascades, and cellular response to IFNγ, while *Spp1/Cd36/Arg1*$^+$ MΦ exhibited angiogenesis functionality. Tissue-resident *Lyz1/Mgl2/Clec4b1*$^+$ MΦ had a gene expression profile enriched for antigen processing and presentation functionality via MHC class II (*SI Appendix*, Fig. S13*B* and Table S1). *Chil3/Plac8/Ly6c2*$^+$Mo exhibited genes enriched for cellular response to IL-4 and positive regulation of TNF biosynthetic process. *Wdfy4/Trim35/Irf8*$^+$ Mo-Dc/Neu showed antigen processing and presentation functionalities (*SI Appendix*, Fig. S13*C*). Collectively, these findings are consistent with FACS data and demonstrate that IA propagates proinflammatory myeloid subsets whereas DAC fortifies anti-inflammatory myeloid populations.

Identification of Differentiation Trajectories of Anti-Inflammatory MΦ Populations and Their Key Transcriptional Regulators. As anti-inflammatory MΦ populations were greatly increased in the mice receiving DAC treatment, pseudotime analysis was conducted in the clusters containing two distinct anti-inflammatory MΦ subsets and their unique functionalities, i.e., *Spp1/Cd36/Arg1*$^+$ MΦ with functionality for angiogenesis (GO:0001525) and *C1qa/Mrc1/Pf4*$^+$ MΦ with functionality for responding to IFNγ (GO:0071346), using *Chil3/Plac8/Ly6c2*$^+$ Mo as the root of lineage trajectories (Fig. 3*A*). Next, genes that are coregulated around trajectory branch points were analyzed to further obtain insights into the genetic profiles governing cell fate decisions. Trajectory branch analysis using Monocle3 identified 22 gen modules that may contribute cell fate specification of *Chil3/Plac8/Ly6c2*$^+$ Mo (*SI Appendix*, Fig. S14). Based on gene expression levels, modules 4 and 9 may contain genes controlling cell fate decision of *Chil3/Plac8/Ly6c2*$^+$ Mo into anti-inflammatory *Spp1/Cd36/Arg1*$^+$ MΦ, while genes in modules 6 and 8 may be responsible for *Chil3/Plac8/Ly6c2*$^+$ Mo into anti-inflammatory *C1qa/Mrc1/Pf4*$^+$ MΦ. We observed increased expression levels of *Arg1*, *Ccl9*, *Crip1*, and *Vegfa* when *Chil3/Plac8/Ly6c2*$^+$ Mo gradually differentiated into *Spp1/Cd36/Arg1*$^+$ MΦ (*SI Appendix*, Fig. S15*A*).

To determine which transcription factors (TFs) may be regulating this differentiation trajectory, we performed the TF binding motif analysis using the RcisTarget R package and TRRUST database. The results indicated that *Sp3*, *Smarcc1*, and *JunD* are the putative key TFs driving this differentiation process with *Smarcc1* and *JunD* having higher expression levels and percentage of cells in *Spp1/Cd36/Arg1*$^+$ MΦ (Fig. 3*B*).

The differentiation of *Chil3/Plac8/Ly6c2*$^+$ Mo into *C1qa/Mrc1/Pf4*$^+$ MΦ was best described by gene modules 6 and 8 (Fig. 3*A* and *SI Appendix*, Fig. S14). This trajectory showed upregulation of *Irf7* and *Stat1* at the later differentiation stage (i.e., *C1qa/Mrc1/Pf4*$^+$ MΦ) (*SI Appendix*, Fig. S15*B*). TF binding motif analysis shows that the primary TFs regulating the differentiation route are *Stat1* and *Bach2* (Fig. 3*C*). Protein–protein network for modules 6 and 8 was also constructed, indicating *Ifit3, Ifit1, Ddx58, Usp18*, and *Isg15* are top 5 nodes with the highest degree and *Stat1-Fyn, Fyn- B2m, B2m-Tap1, Stat1-Ifit3, and Cmpk2-Dck* are top 5 edges with highest betweenness centrality (*SI Appendix*, Fig. S16). In this regard, Stat1 has been shown recently to be required for efficient recruitment of the signaling complex of *Irf8* (45), and lupus GWAS studies indicated that *Irf8* directly interacts with Ifit1 and Stat1, with the latter identified as disease susceptibility gene (46). Since *Irf8* was identified as a potential downstream target and epigenetically modified and activated by

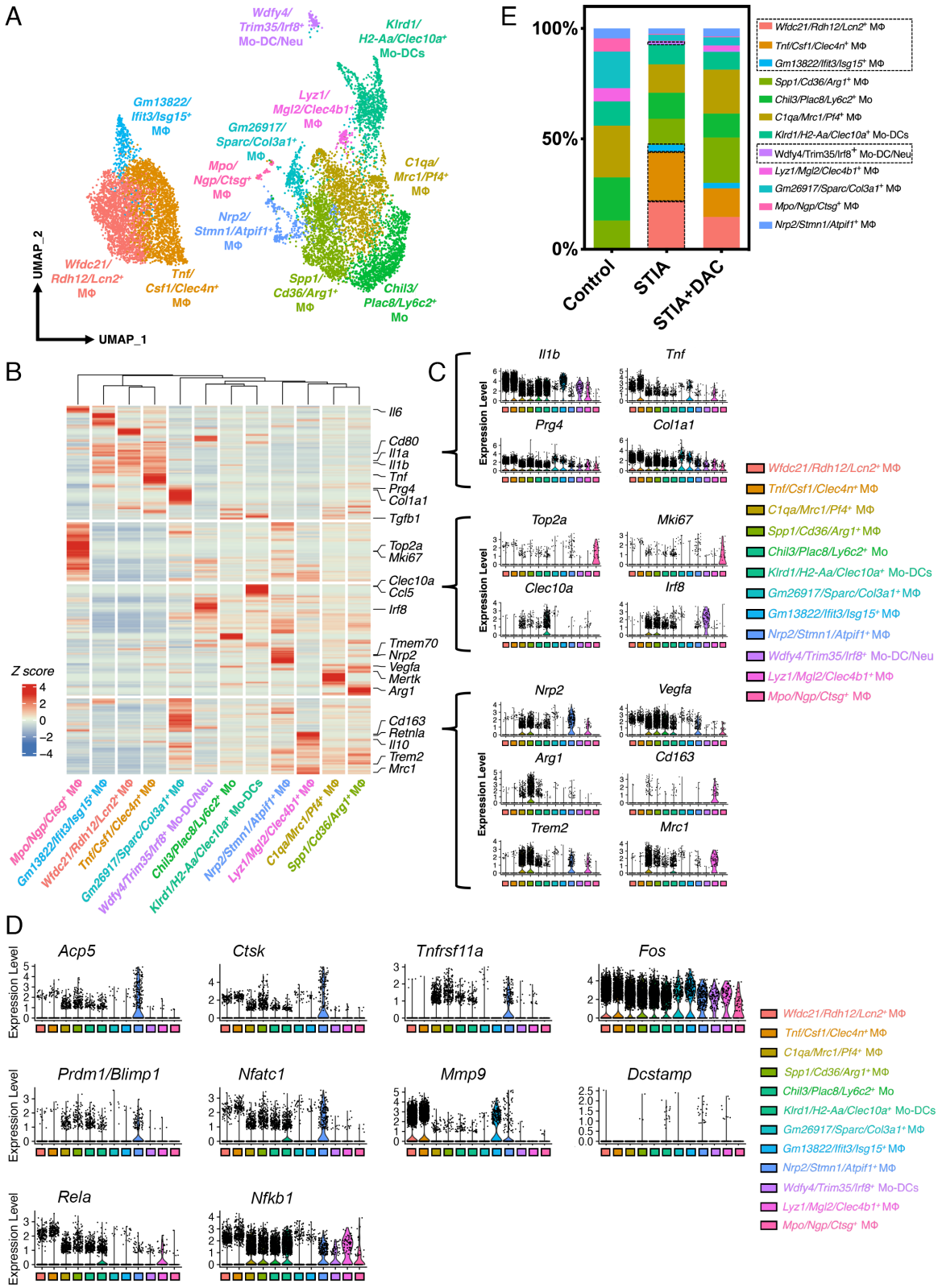

Fig. 2. (*A*) Twelve distinct myeloid cell populations with their specific markers were identified using CCA integration of all myeloid populations from control, STIA, and STIA + DAC mice. (*B–D*) Heatmap and violin plots showing unique transcriptomic profiles defining identified myeloid cell populations and preosteoclasts. (*E*) scRNA-seq analysis showing the changes of myeloid cell populations in the joint synovium harvested from the control, STIA, and STIA + DAC mice. Dashed rectangles indicate populations only observed in the STIA and STIA + DAC mice but not in the control group.

DAC in MΦ, DCs, and neutrophils (26, 31, 34, 47), we further investigated expression levels of *Irf8* in these two anti-inflammatory MΦ populations in control, STIA, and STIA + DAC experimental conditions. DAC treatment significantly promoted both levels and percentage of the cells expressing *Irf7* and *Irf8* in *Spp1/Cd36/Arg1*$^{+}$ MΦ and *C1qa/Mrc1/Pf4*$^{+}$ MΦ populations (Fig. 3*D*).

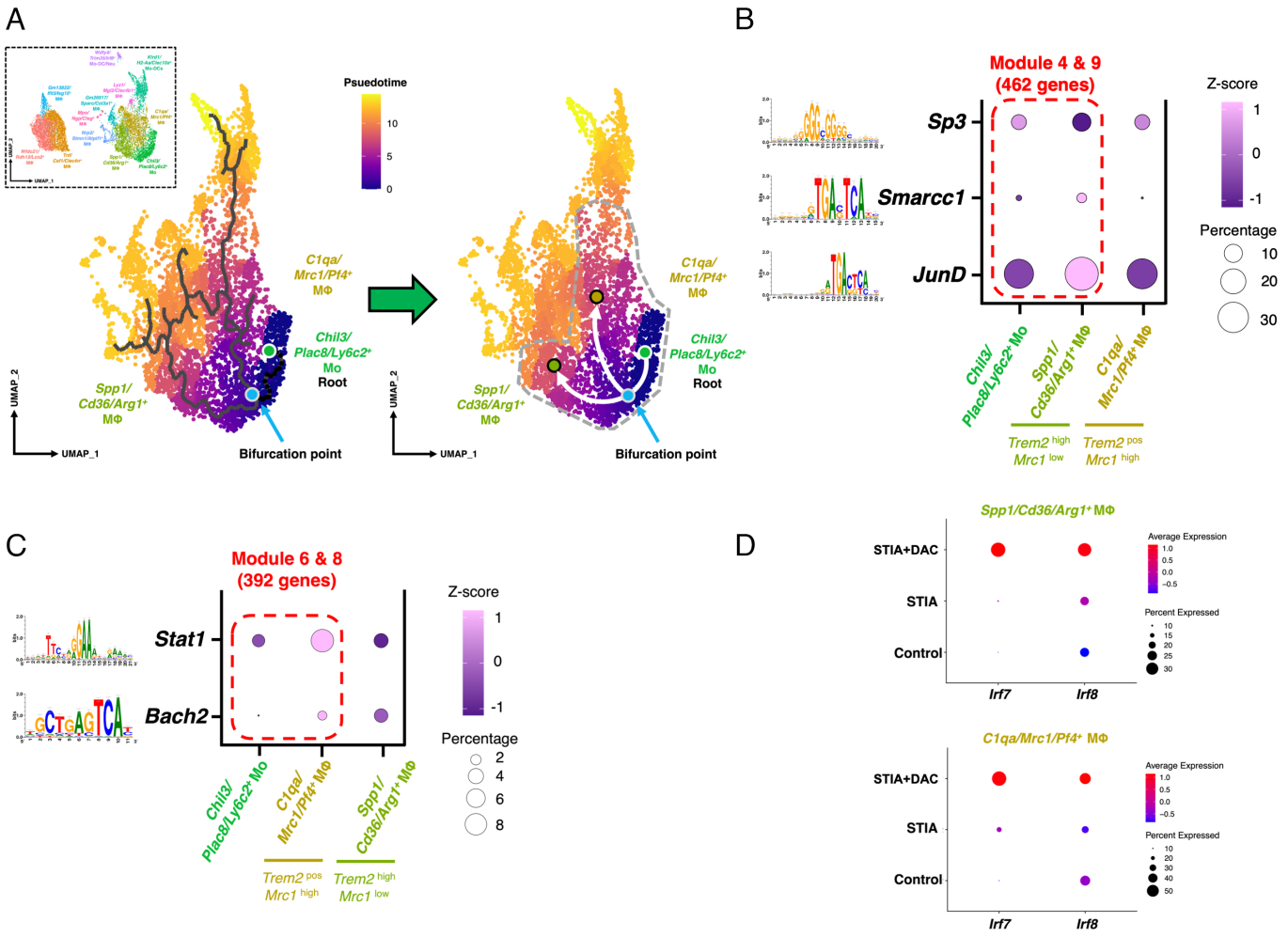

Fig. 3. (*A*) Pseudotime ordering indicates a lineage bifurcation of *Chil3/Plac8/Ly6c2*$^+$ Mo into either anti-inflammatory *Spp1/Cd36/Arg1*$^+$ MΦ or anti-inflammatory *C1qa/Mrc1/Pf4*$^+$ MΦ. (*B*) TF binding motif analysis showing that *Sp3*, *Smarcc1*, and *JunD* are putative TFs regulating differentiation of *Chil3/Plac8/Ly6c2*$^+$ Mo into *Spp1/Cd36/Arg1*$^+$ MΦ. (*C*) *Stat1* and *Bach2* are potential regulators driving *Chil3/Plac8/Ly6c2*$^+$ Mo into *C1qa/Mrc1/Pf4*$^+$ MΦ lineage. (*D*) DAC treatment increased both levels and percentage of the cells expressing *Irf7* and *Irf8* in both *Spp1/Cd36/Arg1*$^+$ MΦ and *C1qa/Mrc1/Pf4*$^+$ MΦ in STIA + DAC mice.

To characterize the phenotype of these cells in vitro, synovial macrophages were collected from WT and Irf8 null mice and subjected ex vivo to ±DAC treatments. Flow cytometry and qPCR were carried out for markers of the two Spp1 and C1qa populations. The data depicted as *SI Appendix*, Fig. S17 show that cells treated with DAC express Mrc1, Arg1, Cq1a, CD36, and Spp1 corroborating the in vivo phenotype.

DAC Caused Major Gene Methylation Changes in IA. Epigenetic regulation has emerged as a hallmark of pathologic states, including IA. To better understand potential therapeutic mechanisms, WGBS was performed on CD11b$^+$ cells isolated from synovial tissues from control mice, STIA mice, and STIA mice after DAC treatment (n = 2 for WGBS per group). Approximately 18 million CpGs assayed at 10× coverage were identified. Comparing control to STIA mice, a significant global increase in CpG methylation was noted (Fig. 4*A*; red graph shift to the right), which was ameliorated by DAC treatment (Fig. 4*B*). Analysis of differentially methylated regions (DMRs) identified 29,808 DMRs between control and STIA mice, 75% of which were hypermethylated, and 25% were hypomethylated (Fig. 4*C*). In comparing STIA mice to DAC-treated STIA mice, a smaller subset of only 773 significant DMRs was identified, with 15% hypermethylated and 85% hypomethylated (Fig. 4*D*). In both comparison groups, methylation changes were noted predominantly within CpG islands (Fig. 4*E*), and DMRs were distributed among gene bodies and intergenic regions (*SI Appendix*, Fig. S15*A*). Pathway analyses on DMRs highlighted peptidyl-tyrosine modification as differently methylated in control vs. STIA mice (*SI Appendix*, Fig. S15*B*), which aligns with the known pathologic role of tyrosine kinases in IA (48). In comparing STIA vs. DAC-treated STIA mice, pathway analysis highlighted broader pathways, including GTPase-mediated signal transduction, focal adhesions, and kinase activity (*SI Appendix*, Fig. S18*B*). We performed gene set enrichment analysis on differentially accessible genes, based on changes in predicted enhancer methylation at nearby loci. In the intersection of genes with both differential accessibility between STIA vs. Ctrl and those with differential expression in STIA vs. STIA + DAC, we identified 34 potentially regulated genes (*SI Appendix*, Table S2). These encompass a range of intronic and distal intergenic regions (*SI Appendix*, Table S2). Gene enrichment analysis reassuringly highlighted overrepresentation of pathways including regulation of bone resorption (by GO Biological Process), NFATC1 signaling (via Elsevier Pathway Collection), and CX3CR1+ cells (by MAGNET 2023) (*SI Appendix*, Fig. S19). The latter is consistent with phenotypic changes in myeloid cells described in our FACS and scRNAseq analyses.

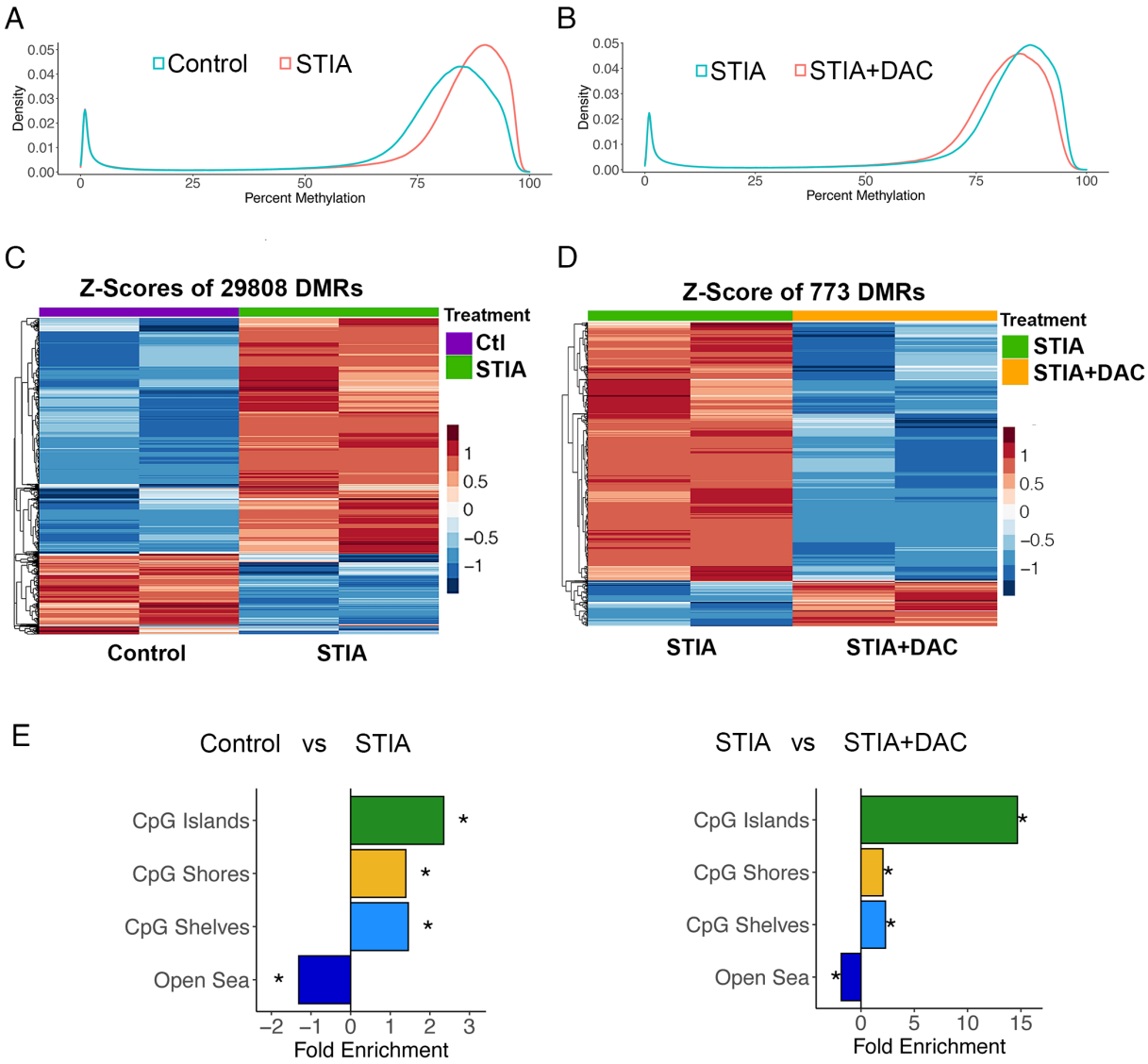

Fig. 4. IA displays significant genomic methylation and the demethylation drug DAC reverses major gene methylation changes. (*A* and *B*) Smoothed single CpG methylation density plots from control vs. STIA mice (*A*) and STIA vs. STIA + DAC (*B*) treated mice, showing overall hypermethylation of STIA mice which is largely reversed by DAC treatment. (*C* and *D*) Heatmaps showing high-level clustering of DMRs in control vs. STIA groups (*C*) (reflecting overall hypermethylation), and STIA vs. STIA + DAC groups (*D*) (reflecting hypomethylation). (*E*) Analysis of DMRs between control vs. STIA and STIA vs. STIA + DAC. Enrichment occurs predominantly at CpG islands, but also at other regions including the open sea.

Irf8 Is Hypomethylated by DAC and Potently Inhibits IA. Our data show that inflammation broadly reprograms gene methylation (Fig. 4) and the anti-inflammatory transcription factor Irf8 is a potential target of DAC (Fig. 3). Therefore, we reasoned that DAC could be working through demethylating inflammation-hypermethylated suppressors, like Irf8, that target myelopoiesis and neutrophilia.

Combining random forest (RF) classifiers and support vector machine algorithm analyses of the top 10% DMRs from our WGBS data, Irf8 was identified among the DAC-regulated genes in STIA, evident by DAC demethylation of Irf8 at CpG islands (Fig. 5*A*). Top regulated DMRs were determined via a generalized least squares regression model including permutation testing of a pooled null distribution, as defined in DMRichR. Analysis of a specific subset of loci for methylation revealed that a region within the *Irf8* promoter is significantly hypomethylated in STIA + DAC mice (Fig. 5*A*). Next, we identified a 485 bp CpG island (DNA methylation/demethylation enzyme binding site, indicated as the green box in *SI Appendix*, Fig. S20*A*) in the murine proximal *Irf8* promoter, which is highly conserved across species (35, 49, 50), confirming that Irf8 is subject to epigenetic regulation.

To validate these findings, we performed the *Irf8* CpG methylation assay targeting this CpG island. Whereas inflammatory signals (LPS and TNF) and RANKL increased methylation (dark blue) of the *Irf8* promoter region in bone marrow macrophages (BMMs) by nearly 25 to 40%, DAC entirely inhibited this methylation (Fig. 5*B*). Even more robust was the staggering 90% *Irf8* CpG methylation observed in $CD11b^+$ cells at the peak of arthritis (dark red), which was drastically prevented by DAC in vivo (Fig. 5*C*). Accordingly, mRNA and protein expression of *Irf8* in synovial $CD11b^+$ cells isolated from ankles of control, STIA, DAC, and DAC-treated STIA mice was diminished under inflammatory conditions (e.g., STIA), whereas treatment with DAC significantly restored or elevated its expression (Fig. 5 *D* and *E* and *SI Appendix*, Fig. S20*B*).

Confirming that Irf8 is a direct target of DAC, the drug failed to inhibit TNFα expression and only slightly inhibited joint swelling in mice lacking Irf8 (LysM -Cre mediated Irf8 deletion).

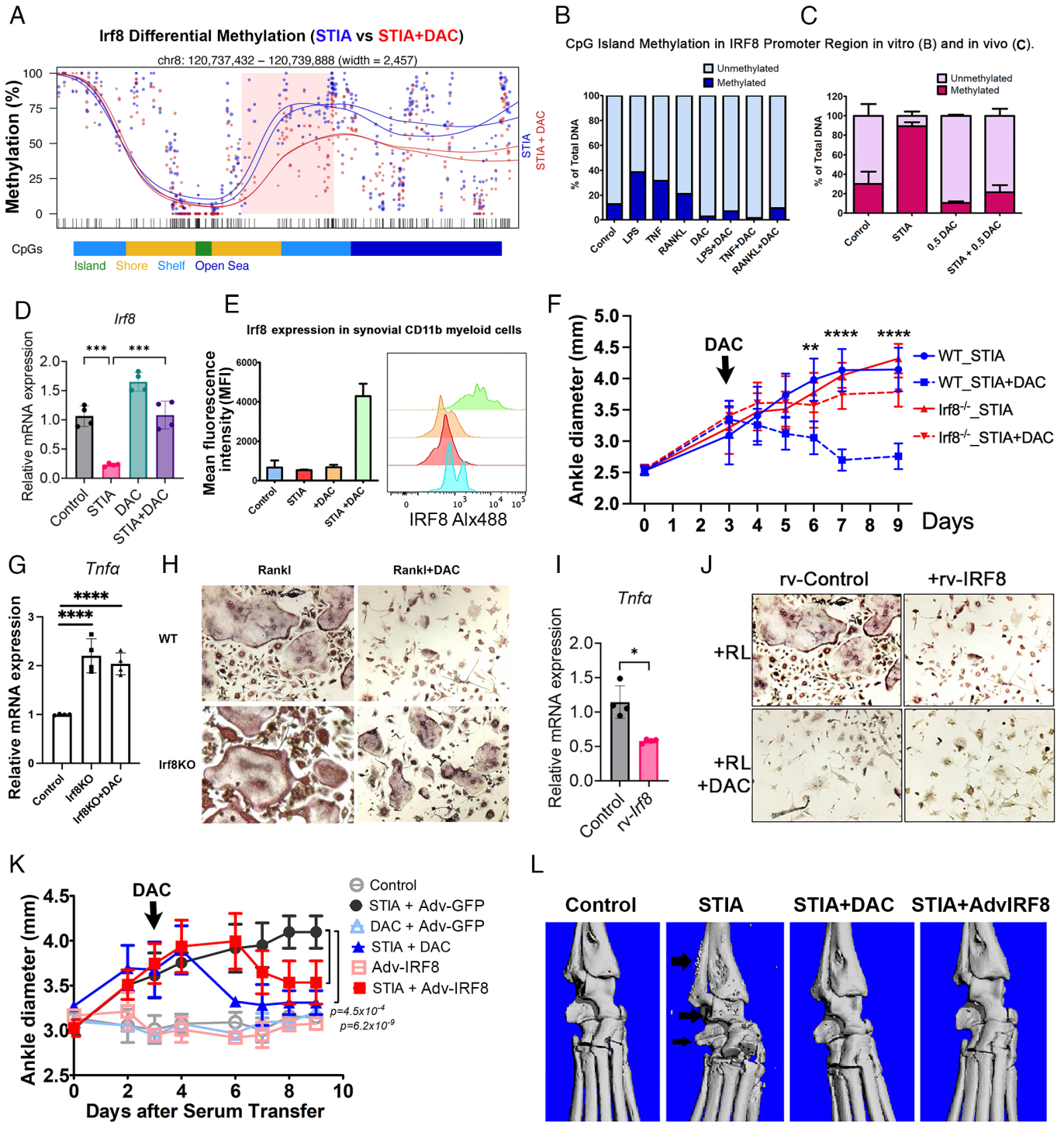

Fig. 5. Irf8 partially mediates the DAC antiosteolytic effect. (*A*) The *Irf8* promoter region is significantly demethylated comparing STIA vs. STIA + DAC. (*B*) One million CD11b$^+$ bone marrow cells were plated on a six-well tissue culture plate and stimulated with either PBS (control), 2 nM DAC, 1 ng/mL LPS, 50 ng/mL TNF, or 100 ng/mL RANKL, with or w/o 2 nM DAC for 24 h. (*C*) CD11b$^+$ cells were isolated from paws of control, STIA ±DAC mice. Genomic DNA was subjected to methylation assay using primers specific to Irf8 CpG island following Qiagen's Methyl II PCR Kit. (*D*) qPCR for *Irf8* fold change compared to control. Error bars represent mean ± SD. One-way ANOVA. ***$P < 0.001$. (*E*) Irf8 protein expression and protein levels (mean fluorescence intensity = MFI) quantified in CD11b$^+$ cells isolated by FACS sorting from the synovium of the various treatment groups. DAC dose in vivo 0.12 mg/kg bw. (*F*) Ankle swelling (diameter) in WT and *Irf8* KO mice subjected to STIA ± DAC. The arrow indicates the starting time of DAC injection in the therapeutic protocol. Two-way ANOVA (Tukey's multiple comparisons test). Error bars represent mean ± SD. Two-way ANONA (Tukey's multiple comparisons test). **$P < 0.01$; ****$P < 0.0001$ WT_STIA+DAC compared with Irf8KO_STIA+DAC. (*G* and *H*) TNFα qPCR and osteoclastogenesis (+RANKL) from WT and Irf8KO cells ±DAC. Error bars represent mean ± SD. One-way ANOVA. ****$P < 0.0001$. (*I* and *J*) TNFα qPCR and osteoclastogenesis from cells expressing retroviral (rv) Irf8 ±DAC. Student's *t* test, *$P < 0.05$. (*K*) Local injection of adenoviral (Adv) Irf8 (10^7 pfu/10 μL) to the joints compared with therapeutic injection of DAC (0.12 mg/kg). Error bars represent mean ± SD. Two-way ANOVA (Tukey's multiple comparisons test). *P* values are indicated in the figure. (*L*) μCT analysis of paws from (*K*).

Furthermore, DAC treatment failed to inhibit osteoclastogenesis in *Irf8* KO (knockout) cells. (Fig. 5 *F*–*H*). More importantly, forced expression of retroviral *Irf8* (*rvIrf8*) in BMMs, mimicking DAC, potently inhibited expression of inflammatory cytokines and osteoclasts (Fig. 5 *I* and *J* and *SI Appendix*, Fig. S20 *C*–*E*). Finally, we tested the potential therapeutic and prophylactic

efficacy of Irf8 in vivo. Adenoviral *Irf8* particles (10^7 pfu/10 μL) were intraarticularly injected in the knee joint space and subcutaneously near the ankle and knee joints of control and STIA mice alongside other groups treated with DAC. Adv-Irf8 robustly inhibited joint swelling in STIA mice nearly comparable to DAC (Fig. 5*K* and *SI Appendix*, Fig. S20*F*). This protective effect was also corroborated with abolishing bone erosion as shown by μCT (Fig. 5*L*). Collectively, these data show that *Irf8* is hypermethylated and inhibited under inflammatory conditions; DAC hypomethylates *Irf8* and induces its expression; virally expressed *Irf8* inhibits inflammatory cytokines, joint swelling, osteoclasts, and bone erosion; and deletion of *Irf8* not only exacerbates osteoclastogenesis and inflammation but also blunts the DAC inhibitory effects on osteoclasts and inflammatory signals. These findings strongly suggest that *Irf8* is among the principal targets of DAC in myeloid cells and is necessary to facilitate DAC actions in these cells.

Discussion

DAC Inhibits Inflammatory Characteristics of Synovial Cells and Ameliorates Murine IA. IA is characterized by hyper-myeloproliferation and neutrophilia (51) underpinned by an exuberant cytokine microenvironment. It is now apparent that cellular, metabolic, and transcriptomic alterations of hematopoietic progenitors that elicit proinflammatory phenotype are at the crux of this process (52). Likewise, the inflammatory milieu reprograms synovial FBs, CD4+ and CD8+ T cells—primarily T regulatory cells—and impedes their protective and regenerative functions (53, 54). Under inflammatory conditions, the genomes of myeloid, lymphoid, and several other cell types undergo hypermethylation that hinders homeostatic functions by dampening cellular suppressors and exacerbating disease pathology (5, 6, 55, 56). Therefore, we surmised that hypomethylating agents hold promise to reactivate methylated suppressor genes (57) and restore tissue homeostasis. Using several mouse models of arthritis, we first demonstrate that IA is accentuated by exacerbated myeloproliferation and neutrophilia. Specifically, FACS and transcriptomic analyses demonstrate increased propensity of proinflammatory (M1 type) MΦ, atypical LyC6$^+$ MΦ, Ly6G$^+$ neutrophils, Trem2$^-$, Cx3cr1$^-$ proinflammatory MΦ, Pdpn$^+$Fapα$^+$ FBs, and reprogramming of Foxp3$^+$ T_{REGS} into Rorγgt$^+$ T_H17 pathogenic cells. Furthermore, we noted a significant increase in RANK$^+$ progenitors that are hypersensitive to RANKL and drive the osteolytic process. Remarkably, administration of the low dose of the hypomethylation drug DAC reversed these in vitro cellular changes and restored cellular homeostasis. Even more convincingly, administration of low doses of DAC in vivo ameliorated IA in STIA, CIA, and CAIA mouse models and therapeutically restored tissue homeostasis, highlighting the detrimental role of inflammatory macrophages, neutrophils, pathogenic T helper cells, and activated synovial FBs. These findings are supported by previous evidence wherein DAC and 5-azacitidine efficiently altered experimental IA pathogenesis (42, 58–60).

DAC Reduced Myeloid Cell Clusters in the Synovium and Modified Their Transcriptomic Signature. Significant strides have been made to identify unique synovial cell clusters to advance joint therapy (61, 62). In this regard, joint homeostasis is governed by tissue-resident MΦ (Trem2$^+$ and Cx3cr1$^+$), lining layer, and sublining fibroblasts (Pdpn$^+$) that together form protective cellular barriers in the joint (63). We carried out scRNA-seq studies and identified 12 cell clusters reflecting the heterogeneity of synovial cells. Notably, the inflammatory phenotype of these clusters elicited by IA was largely curbed in the presence of DAC through restoration of their homeostatic anti-inflammatory phenotype (MerTK$^+$, CD206$^+$, CD163$^+$, and Cx3cr1$^+$). These changes were corroborated by diminished or complete prevention of IA features in mice.

Our scRNA-seq analysis revealed that DAC dramatically reduced myeloid cell populations in STIA joints. In total, 12 unique myeloid populations were detected in the synovium across all treatment groups, of which four proinflammatory groups were present only in the arthritic joints, whereas DAC-treated STIA mice exhibited an increased percentage of five anti-inflammatory macrophage populations compared to arthritic mice. Of interest, expression of members of the TAM family receptor tyrosine kinase MER (MerTK) is diminished in IA, yet treatment with DAC restores its expression and its anti-inflammatory signature highlighted by elevated expression of IL-10, as has been also shown previously (63–65). Additional work is required to establish the potential anti-inflammatory role of MerTK$^+$ in IA. Similar changes in Trem2 were also observed. We also noted significant changes in the expression of Cx3cr1, a recently reported marker of specialized tissue-resident MΦ that form immunological barrier at the synovial lining to protect the joint (66). IA-induced reduction of Cx3cr1 expression was significantly restored following exposure to DAC. Of special note, we identified clusters expressing *Isg15*, *Clec10a*, and *Clec4b1* with previously undescribed roles in IA pathogenesis. In this regard, we have recently unveiled that *Isg15* is an essential regulator of osteoclasts (67) and inflammatory osteolysis (39). In addition, we report a unique tissue-residing *Lyz1/Mgl2/Clec4b1*$^+$ MΦ subset, which has the highest expression levels of *Cd81*, *Cd163,* and *Il10* among all MΦ populations. This cell population which is characterized by expression of galactose/GalNa-c-lectin (MGL) (68) and FcγR-coupled C-lectin receptor dendritic cell immune-activating receptor (Clec4b1) (69) displays immunomodulatory properties through induction of protective T cell responses to resolve inflammation (69). Additional studies are required to delineate the role of Clec4b1 and Clec10a in IA.

Collectively, these findings suggest that DAC acts systemically and at the local joint environment to rewire homeostatic immune and anti-inflammatory activities of tissue-resident and synovium-infiltrating cells. More importantly, DAC appears to restore tissue homeostasis by reversing the inflammatory phenotype of multiple cell types including myeloid, lymphoid, SFs, and potentially other cell types. Transcriptomic profiling further identified three inflammatory populations responsive to IFNγ and IL-1. On the other hand, transcriptomic signature and GO term functional analysis of other clusters revealed cellular responses including regulation of ERK signaling, angiogenesis, antigen processing, fibrosis, collagen fibril organization, and efferocytosis. These findings suggest that DAC regulates a wide array of cell functions including cell cycle, mitochondrial function, cytokine responsiveness, immune regulation, and tissue remodeling. At the transcription factor level, DAC appears to regulate specific TFs including *Stat1, Bach2, Irf7*, and *Irf8* in late-stage differentiation of Mrc1$^+$ and Arg1$^+$ anti-inflammatory macrophage populations, as discussed below.

Hypomethylation by DAC Restores Suppressor Gene Function. Our study demonstrates that IA dramatically hypermethylates the genome of synovial cells leading to pathogenic phenotypes, consistent with recent reports (3, 10, 15, 70, 71). We identified hypermethylation of the suppressor gene *Irf8* as a key therapeutic target. Our focus on Irf8 as a potential modulator of DAC-induced inhibition of IA is supported by evidence pointing to its potent role as modulator of myelopoiesis and neutrophilia, and that hypermethylation of Irf8 or lack of Irf8 promotes neutrophilia and osteoclastogenesis (25, 30, 31, 36, 72), whereas

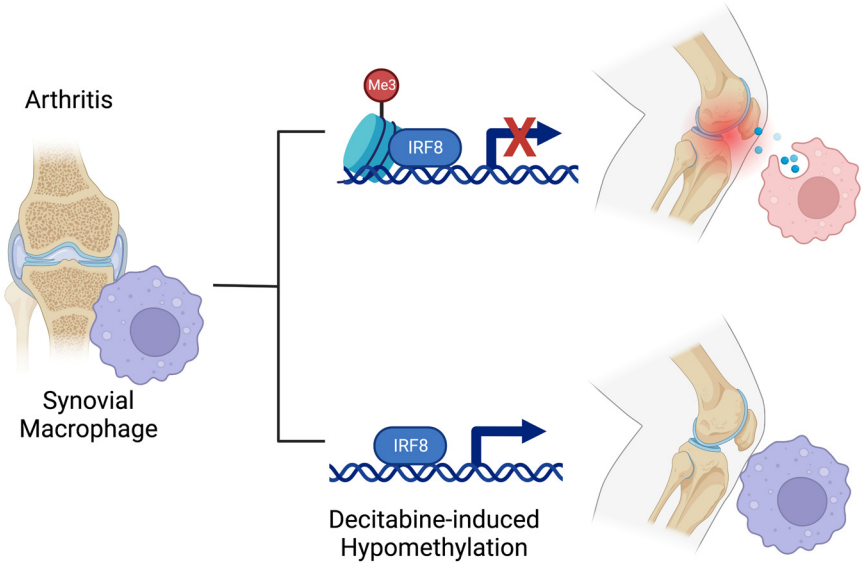

Fig. 6. Summary graphical model. IA induces hypermethylation and inhibition of the suppressor function of Irf8 resulting with joint swelling, synovitis, and tissue degradation. Administration of the hypomethylating agent DAC reactivates Irf8 leading to inhibition of joint inflammation.

hypomethylation of Irf8 increases Irf8 expression and activity, and suppresses neutrophil differentiation in C/EBPα-dependent manner (31, 37). Hence, we hypothesized that inflammation blunts expression of suppressive factor Irf8 via hypermethylating its promoter region leading to myeloid proliferation, neutrophilia, and RA propagation. We also surmised that demethylation of Irf8 by DAC may enable reprogramming of myeloid differentiation to resolve IA. Indeed, our transcriptomic studies unveiled several Irf8-expressing myeloid populations. Wdyf4/Trim35/Irf8+ Mo-Dc/Neu cells have the highest expression of Irf8. We also show that two anti-inflammatory macrophages (C1aq/Mcr1/Pf4 and Spp1/Cd36/Arg1) have strong Irf8 expression (Fig. 2*B*; Irf8 violin plot). These two populations were largely increased in the STIA + DAC group (55.3% and 74%, respectively). It is noteworthy that Spp1 and Mrc1 have been associated with reparative and regenerative anti-inflammatory macrophages (73, 74).

Our data indicate that DAC demethylates STIA-induced hypermethylation of the genome and *Irf8* promoter regions. More importantly, DAC restores Irf8 protein expression in myeloid cells from STIA mice, inhibits osteoclastogenesis, and most notably, Irf8 mediates the DAC effect and directly inhibits IA inflammatory and erosive characteristics. These findings are consistent with the established antiosteoclast function of Irf8 (37, 72, 75, 76). It remains unclear whether DAC targets Irf8 directly or through proximal regulators. BATF, which was among the highest expressed TFs we detected, has been shown to sustain Irf8 autoactivation (35), suggesting that it is a potential target of DAC. Further, our observation that DAC regulates a unique PU.1 expressing cluster substantiates studies wherein binding of the primary myeloid transcription factor *PU.1* and the osteoclast TF *Nfatc1* with Irf8 binding sites in myeloid progenitors and differentiated OCs were described (77), with evidence that Irf8 regulates Nfatc1 expression (72, 77, 78). Furthermore, we detected upregulation of STAT1 in C1aq/Mcr1/Pf4 anti-inflammatory macrophages. In this regard, recent studies have shown that STAT1 is required for efficient Irf8 signaling complex assembly and function (45) and a lupus GWAS showed that Irf8 directly binds to Ifit1 and Stat1, the latter identified as disease susceptibility gene (46). Thus, STAT1-Irf8 complex is potentially required for DAC-induced differentiation of Chil3/Plac8/Ly6c2+ monocytes into C1aq/Mcr1/Pf4 anti-inflammatory macrophages. Our transcriptomic studies also demonstrated expression of JunD, a transcription factor that has been shown to limit expression of Irf8 (79). Consistently**,** recent studies have shown that JunD is hypermethylated and its expression is down-regulated under inflammatory conditions. Conversely, overexpression of JunD elicited an anti-inflammatory response (80).

Collectively, these observations suggest that the Irf8 regulatory network is far more elaborate than anticipated. Therefore, Irf8 appears as a central intersection point for several regulatory elements, and hence, it is not surprising that re-expression of Irf8 directly or through DAC-mediated hypomethylation overrides proximal suppressions and inhibits inflammation and bone erosion in IA (Fig. 6).

Materials and Methods

Note: Additional methodology is included in *SI Appendix* section.

Study Design. The objective of this study was to determine the efficacy of DAC and IRF8 in the treatment of murine IA. Mice were randomly assigned to experimental groups of the different arthritis models. The sample size was determined based on prior experience with penetrance of each model. Outliers were included in the final calculations. This study utilized a low dose of DAC and demonstrated its efficacy and nontoxic effect in vitro and in vivo. All experiments reflect a minimum of five independent biological replicates. Investigators were blinded to the experimental groups and data was assessed by at least three independent investigators.

Statistical Analysis. Male and female mice were used at equal ratios. All experiments represent biological replicates and were repeated at least three times, unless otherwise stated. Statistical analyses were performed using appropriate statistical tests using GraphPad Prism v9. All graphs were generated using Prism as well. Multiple treatments were analyzed by one-way or two-way ANOVA followed by Tukey's test multiple comparisons test. Student's *t* test was used for comparing two groups. *P* values are indicated where applicable. $*P < 0.05$, $**P < 0.01$, $***P < 0.0005$, and $****P < 0.0001$. Mouse activity and pain measurements, osteoclast counts, and immunostaining data were scored by investigators blinded to the experimental conditions.

Data, Materials, and Software Availability. Transcriptomic dataset is available in NCBI GEO (81).

ACKNOWLEDGMENTS. This work is supported by NIH grant R01-AR072623 (Y.A.-A.), NIH grant R01-AR082192 (Y.A.-A.), Biomedical grant from Shriners Hospital for Children (Y.A.-A.), P30 AR074992 NIH Core Center for Musculoskeletal Biology and Medicine (Y.A.-A.), NIH grants R01-AR076758, R01 AG077732, and R01-AI161022 (to G.M.), NIH T32 DK007120 (N.P.S.), NIH K99/R00- AR075899, and Orthopedic Research and Education Foundation (C.-L.W.).

Author affiliations: [a]Department of Orthopedic Surgery, Washington University School of Medicine, St. Louis, MO 63110; [b]Department of Medicine, Washington University School of Medicine, St. Louis, MO 63110; [c]Department of Emergency Medicine, Washington University School of Medicine, St. Louis, MO 63110; [d]HealthSpan Technologies, Inc, St. Louis, MO 63110; [e]Department of Orthopedics and Physical Performance, University of Rochester, Rochester, NY 14642; [f]Department of Cell Biology and Physiology, Washington University School of Medicine, St. Louis, MO 63110; and [g]Shriners Hospital for Children, St. Louis, MO 63110

1. K. A. Oduro Jr. *et al.*, Myeloid skewing in murine autoimmune arthritis occurs in hematopoietic stem and primitive progenitor cells. *Blood* **120**, 2203–2213 (2012).
2. T. H. Chen, G. Swarnkar, G. Mbalaviele, Y. Abu-Amer, Myeloid lineage skewing due to exacerbated NF-kappaB signaling facilitates osteopenia in Scurfy mice. *Cell Death Dis.* **6**, e1723 (2015).
3. F. L. Yuan, X. Li, R. S. Xu, D. L. Jiang, X. G. Zhou, DNA methylation: Roles in rheumatoid arthritis. *Cell Biochem. Biophys.* **70**, 77–82 (2014).
4. M. Alimohammadi *et al.*, DNA methylation changes and inflammaging in aging-associated diseases. *Epigenomics* **14**, 965–986 (2022).
5. L. Kang, H. Zhang, C. Jia, R. Zhang, C. Shen, Epigenetic modifications of inflammation in intervertebral disc degeneration. *Ageing Res. Rev.* **87**, 101902 (2023).
6. S. Zhang *et al.*, Targeting epigenetic regulators for inflammation: Mechanisms and intervention therapy. *MedComm* **3**, e173 (2022).
7. E. Ballestar, T. Li, New insights into the epigenetics of inflammatory rheumatic diseases. *Nat. Rev. Rheumatol.* **13**, 593–605 (2017).
8. B. Rhead *et al.*, Rheumatoid arthritis naive T cells share hypermethylation sites with synoviocytes. *Arthritis Rheumatol.* **69**, 550–559 (2017).
9. D. Hammaker *et al.*, LBH gene transcription regulation by the interplay of an enhancer risk allele and DNA methylation in rheumatoid arthritis. *Arthritis Rheumatol.* **68**, 2637–2645 (2016).
10. Y. Liu *et al.*, Epigenome-wide association data implicate DNA methylation as an intermediary of genetic risk in rheumatoid arthritis. *Nat. Biotechnol.* **31**, 142–147 (2013).
11. S. Viatte, D. Plant, S. Raychaudhuri, Genetics and epigenetics of rheumatoid arthritis. *Nat. Rev. Rheumatol.* **9**, 141–153 (2013).
12. K. Klein, C. Ospelt, S. Gay, Epigenetic contributions in the development of rheumatoid arthritis. *Arthritis Res. Ther.* **14**, 227 (2012).
13. T. T. Glant, K. Mikecz, T. A. Rauch, Epigenetics in the pathogenesis of rheumatoid arthritis. *BMC Med.* **12**, 35 (2014).
14. C. Angiolilli *et al.*, Inflammatory cytokines epigenetically regulate rheumatoid arthritis fibroblast-like synoviocyte activation by suppressing HDAC5 expression. *Ann. Rheum Dis.* **75**, 430–438 (2016).
15. K. Nakano, D. L. Boyle, G. S. Firestein, Regulation of DNA methylation in rheumatoid arthritis synoviocytes. *J. Immunol.* **190**, 1297–1303 (2013).
16. S. Hagemann, O. Heil, F. Lyko, B. Brueckner, Azacytidine and decitabine induce gene-specific and non-random DNA demethylation in human cancer cell lines. *PLoS One* **6**, e17388 (2011).
17. J. Nie, L. Liu, X. Li, W. Han, Decitabine, a new star in epigenetic therapy: The clinical application and biological mechanism in solid tumors. *Cancer Lett.* **354**, 12–20 (2014).
18. H. Li *et al.*, Very-low-dose decitabine is effective in treating intermediate- or high-risk myelodysplastic syndrome. *Acta Haematol.* **138**, 168–174 (2017).
19. W. Wu *et al.*, Low-dose decitabine plus all-trans retinoic acid in patients with myeloid neoplasms ineligible for intensive chemotherapy. *Ann. Hematol.* **95**, 1051–1057 (2016).
20. J. Jasielec, V. Saloura, L. A. Godley, The mechanistic role of DNA methylation in myeloid leukemogenesis. *Leukemia* **28**, 1765–1773 (2014).
21. K. Agrawal, V. Das, P. Vyas, M. Hajduch, Nucleosidic DNA demethylating epigenetic drugs–A comprehensive review from discovery to clinic. *Pharmacol. Ther.* **188**, 45–79 (2018).
22. E. A. Griffiths, S. D. Gore, DNA methyltransferase and histone deacetylase inhibitors in the treatment of myelodysplastic syndromes. *Semin. Hematol.* **45**, 23–30 (2008).
23. V. Singh, P. Sharma, N. Capalash, DNA methyltransferase-1 inhibitors as epigenetic therapy for cancer. *Curr. Cancer Drug Targets* **13**, 379–399 (2013).
24. P. Wijermans *et al.*, Low-dose 5-aza-2′-deoxycytidine, a DNA hypomethylating agent, for the treatment of high-risk myelodysplastic syndrome: A multicenter phase II study in elderly patients. *J. Clin. Oncol.* **18**, 956–962 (2000).
25. T. Holtschke *et al.*, Immunodeficiency and chronic myelogenous leukemia-like syndrome in mice with a targeted mutation of the ICSBP gene. *Cell* **87**, 307–317 (1996).
26. G. E. Grajales-Reyes *et al.*, Batf3 maintains autoactivation of Irf8 for commitment of a CD8alpha(+) conventional DC clonogenic progenitor. *Nat. Immunol.* **16**, 708–717 (2015).
27. K. M. Murphy, Transcriptional control of dendritic cell development. *Adv. Immunol.* **120**, 239–267 (2013).
28. D. J. Theisen *et al.*, Batf3-dependent genes control tumor rejection induced by dendritic cells independently of cross-presentation. *Cancer Immunol. Res.* **7**, 29–39 (2019).
29. T. Tamura, T. Nagamura-Inoue, Z. Shmeltzer, T. Kuwata, K. Ozato, ICSBP directs bipotential myeloid progenitor cells to differentiate into mature macrophages. *Immunity* **13**, 155–165 (2000).
30. D. Kurotaki *et al.*, IRF8 inhibits C/EBPalpha activity to restrain mononuclear phagocyte progenitors from differentiating into neutrophils. *Nat. Commun.* **5**, 4978 (2014).
31. T. Tamura, D. Kurotaki, S. Koizumi, Regulation of myelopoiesis by the transcription factor IRF8. *Int. J. Hematol.* **101**, 342–351 (2015).
32. M. Scheller *et al.*, Altered development and cytokine responses of myeloid progenitors in the absence of transcription factor, interferon consensus sequence binding protein. *Blood* **94**, 3764–3771 (1999).
33. H. Tsujimura, T. Nagamura-Inoue, T. Tamura, K. Ozato, IFN consensus sequence binding protein/IFN regulatory factor-8 guides bone marrow progenitor cells toward the macrophage lineage. *J. Immunol.* **169**, 1261–1269 (2002).
34. A. Yanez, M. Y. Ng, N. Hassanzadeh-Kiabi, H. S. Goodridge, IRF8 acts in lineage-committed rather than oligopotent progenitors to control neutrophil vs monocyte production. *Blood* **125**, 1452–1459 (2015).
35. D. Kurotaki *et al.*, Transcription factor IRF8 governs enhancer landscape dynamics in mononuclear phagocyte progenitors. *Cell Rep.* **22**, 2628–2641 (2018).
36. C. Fang *et al.*, Cutting edge: EZH2 promotes osteoclastogenesis by epigenetic silencing of the negative regulator IRF8. *J. Immunol.* **196**, 4452–4456 (2016).
37. B. Zhao *et al.*, Interferon regulatory factor-8 regulates bone metabolism by suppressing osteoclastogenesis. *Nat. Med.* **15**, 1066–1071 (2009).
38. V. Rishi *et al.*, CpG methylation of half-CRE sequences creates C/EBPalpha binding sites that activate some tissue-specific genes. *Proc. Natl. Acad. Sci. U.S.A.* **107**, 20311–20316 (2010).
39. N. S. Adapala *et al.*, Inflammatory osteolysis is regulated by site-specific ISGylation of the scaffold protein NEMO. *Elife* **9**, e56095 (2020).
40. K. R. Aupperle *et al.*, NF-kB regulation by IkB kinase-2 in rheumatoid arthritis synoviocytes. *J. Immunol.* **166**, 2705–2711 (2001).
41. S. Dai, T. Hirayama, S. Abbas, Y. Abu-Amer, The IkappaB kinase (IKK) inhibitor, NEMO-binding domain peptide, blocks osteoclastogenesis and bone erosion in inflammatory arthritis. *J. Biol. Chem.* **279**, 37219–37222 (2004).
42. Y.-S. Huang *et al.*, Pharmacological modulation of T cell immunity results in long-term remission of autoimmune arthritis. *Proc. Natl. Acad. Sci. U.S.A.* **118**, e2100939118 (2021).
43. S. Landman *et al.*, Immune responses to azacytidine in animal models of inflammatory disorders: A systematic review. *J. Transl. Med.* **19**, 11 (2021).
44. N. S. Harasymowicz *et al.*, Single-cell RNA sequencing reveals the induction of novel myeloid and myeloid-associated cell populations in visceral fat with long-term obesity. *FASEB J.* **35**, e21417 (2021).
45. M. Parrini *et al.*, The C-terminal transactivation domain of STAT1 has a gene-specific role in transactivation and cofactor recruitment. *Front. immunol.* **9**, 2879 (2018).
46. T. Sezin *et al.*, Gene expression analysis reveals novel shared gene signatures and candidate molecular mechanisms between pemphigus and systemic lupus erythematosus in CD4(+) T cells. *Front. Immunol.* **8**, 1992 (2017).
47. M. L. Ibrahim *et al.*, Myeloid-derived suppressor cells produce IL-10 to elicit DNMT3b-dependent IRF8 silencing to promote colitis-associated colon tumorigenesis. *Cell Rep.* **25**, 3036–3046.e6 (2018).
48. P. E. Palominos, I. B. Lineburger, R. M. Xavier, Emerging protein kinase inhibitors for the treatment of rheumatoid arthritis. *Expert Opin. Emerg. Drugs* **26**, 303–321 (2021).
49. V. Durai *et al.*, Cryptic activation of an Irf8 enhancer governs cDC1 fate specification. *Nat. Immunol.* **20**, 1161–1173 (2019).
50. K. C. Zhu *et al.*, Functional characterization of IRF8 regulation of type II IFN in golden pompano (Trachinotus ovatus). *Fish Shellfish Immunol.* **94**, 1–9 (2019).
51. W. Chen, Q. Wang, Y. Ke, J. Lin, Neutrophil function in an inflammatory milieu of rheumatoid arthritis. *J. Immunol. Res.* **2018**, 8549329 (2018).
52. I. Mitroulis *et al.*, Modulation of myelopoiesis progenitors is an integral component of trained immunity. *Cell* **172**, 147–161.e12 (2018).
53. S. Lindley *et al.*, Defective suppressor function in CD4(+)CD25(+) T-cells from patients with type 1 diabetes. *Diabetes* **54**, 92–99 (2005).
54. S. Floess *et al.*, Epigenetic control of the foxp3 locus in regulatory T cells. *PLoS Biol.* **5**, e38 (2007).
55. J. Shen, Y. Abu-Amer, R. J. O'Keefe, A. McAlinden, Inflammation and epigenetic regulation in osteoarthritis. *Connect. Tissue Res.* **58**, 49–63 (2017).
56. L. Falkowski, J. Buddenkotte, A. Datsi, Epigenetics in T-cell driven inflammation and cancer. *Semin. Cell Dev. Biol.* **154**, 250–260 (2023).
57. S. S. Palii, B. O. Van Emburgh, U. T. Sankpal, K. D. Brown, K. D. Robertson, DNA methylation inhibitor 5-Aza-2′-deoxycytidine induces reversible genome-wide DNA damage that is distinctly influenced by DNA methyltransferases 1 and 3B. *Mol. Cell Biol.* **28**, 752–771 (2008).
58. H. Kröger, A. Dietrich, R. Grätz, A. Wild, W. Ehrlich, The effect of tryptophan plus methionine, 5-azacytidine, and methotrexate on adjuvant arthritis of rat. *Gen. Pharmacol.* **33**, 195–201 (1999).
59. M. C. Petralia *et al.*, Effects of treatment with the hypomethylating agent 5-aza-2′-deoxycytidine in murine type II collagen-induced arthritis. *Pharmaceuticals* **12**, 174 (2019).
60. D. M. Tóth *et al.*, Amelioration of autoimmune arthritis in mice treated with the DNA methyltransferase inhibitor 5′-azacytidine. *Arthritis Rheumatol.* **71**, 1265–1275 (2019).
61. A. P. Croft *et al.*, Distinct fibroblast subsets drive inflammation and damage in arthritis. *Nature* **570**, 246–251 (2019).
62. J. S. Smolen *et al.*, Rheumatoid arthritis. *Nat. Rev. Dis. Primers* **4**, 18001 (2018).
63. S. Alivernini *et al.*, Distinct synovial tissue macrophage subsets regulate inflammation and remission in rheumatoid arthritis. *Nat. Med.* **26**, 1295–1306 (2020).
64. C. V. Rothlin, S. Ghosh, E. I. Zuniga, M. B. Oldstone, G. Lemke, TAM receptors are pleiotropic inhibitors of the innate immune response. *Cell* **131**, 1124–1136 (2007).
65. C. E. J. Waterborg *et al.*, Protective role of the MER tyrosine kinase via efferocytosis in rheumatoid arthritis models. *Front. Immunol.* **9**, 742 (2018).
66. S. Culemann *et al.*, Locally renewing resident synovial macrophages provide a protective barrier for the joint. *Nature* **572**, 670–675 (2019).
67. S. MacLauchlan *et al.*, STING-dependent interferon signatures restrict osteoclast differentiation and bone loss in mice. *Proc. Natl. Acad. Sci. U.S.A.* **120**, e2210409120 (2023).
68. V. D. Costa *et al.*, Lung tumor cells with different Tn antigen expression present distinctive immunomodulatory properties. *Int. J. Mol. Sci.* **23**, 12047 (2022).
69. K. Toyonaga *et al.*, C-type lectin receptor DCAR recognizes mycobacterial phosphatidyl-inositol mannosides to promote a Th1 response during infection. *Immunity* **45**, 1245–1257 (2016).
70. C. E. McCall, B. Yoza, T. Liu, M. El Gazzar, Gene-specific epigenetic regulation in serious infections with systemic inflammation. *J. Innate Immun.* **2**, 395–405 (2010).
71. C. Yang *et al.*, Epigenetic regulation in the pathogenesis of rheumatoid arthritis. *Front. Immunol.* **13**, 859400 (2022).

72. A. Das *et al.*, Monocyte subsets with high osteoclastogenic potential and their epigenetic regulation orchestrated by IRF8. *J. Bone Miner. Res.* **36**, 199–214 (2021).
73. K. Shirakawa *et al.*, MerTK expression and ERK activation are essential for the functional maturation of osteopontin-producing reparative macrophages after myocardial infarction. *J. Am. Heart Assoc.* **9**, e017071 (2020).
74. R. Bill *et al.*, CXCL9:SPP1 macrophage polarity identifies a network of cellular programs that control human cancers. *Science* **381**, 515–524 (2023).
75. H. Xu *et al.*, Notch-RBP-J signaling regulates the transcription factor IRF8 to promote inflammatory macrophage polarization. *Nat. Immunol.* **13**, 642–650 (2012).
76. B. Zhao, S. N. Grimes, S. Li, X. Hu, L. B. Ivashkiv, TNF-induced osteoclastogenesis and inflammatory bone resorption are inhibited by transcription factor RBP-J. *J. Exp. Med.* **209**, 319–334 (2012).
77. N. Izawa *et al.*, Cooperation of PU.1 with IRF8 and NFATc1 defines chromatin landscapes during RANKL-induced osteoclastogenesis. *J. Bone Miner. Res.* **34**, 1143–1154 (2019).
78. J. Wang *et al.*, ASP2-1, a polysaccharide from Acorus tatarinowii Schott, inhibits osteoclastogenesis via modulation of NFATc1 and attenuates LPS-induced bone loss in mice. *Int. J. Biol. Macromol.* **165**, 2219–2230 (2020).
79. T. M. Carr, J. D. Wheaton, G. M. Houtz, M. Ciofani, JunB promotes Th17 cell identity and restrains alternative CD4(+)T-cell programs during inflammation. *Nat. Commun.* **8**, 301 (2017).
80. S. Hussain *et al.*, Hyperglycemia induces myocardial dysfunction via epigenetic regulation of JunD. *Circ. Res.* **127**, 1261–1273 (2020).
81. G. Swarnkar *et al.*, Data from "DNA hypomethylation ameliorates erosive inflammatory arthritis by modulating interferon regulatory factor-8." NCBI GEO. https://www.ncbi.nlm.nih.gov/geo/query/acc.cgi?acc=GSM8031356. Deposited 23 January 2024.